



Article

Quantitative Representation of Dynamic Mechanical Properties and Internal Damage in Deep-Seated Damaged Granite

Luyang Chen ¹, Huaibao Chu ^{1,*}, Donghui Wang ^{2,*}, Bo Sun ¹ , Zilong Wen ¹ and Haixia Wei ¹ 

¹ School of Civil Engineering, Henan Polytechnic University, Jiaozuo 454003, China; chenluyang2022@163.com (L.C.); bosun0419@163.com (B.S.)

² The Second Company of China Construction Second Engrg Bureau Ltd., Shenzhen 518066, China

* Correspondence: chuhuaibao@hpu.edu.cn (H.C.); wdh1661893127@163.com (D.W.)

Abstract: Understanding the dynamics of damaged rock masses and the evolution of internal fractures is beneficial to the construction of deep engineering projects. Dynamic tests on damaged granite were carried out using a split Hopkinson device which can apply a confining pressure. A group of damaged granites was CT-scanned and three-dimensional reconstructed using Avizo 2020.1 software. The results indicate that with increasing damage, the peak stress and peak modulus of the damaged granite decrease, while the peak strain increases. When the initial damage is consistent, all three parameters increase with the increasing confining pressure. Confining pressure alters the number and development direction of internal fissures in granite. Higher confining pressure results in fewer fissures, with their development direction shifting more towards the center of the sample and becoming straighter. The total volume of fissures within the rock samples, the volume of through fissures, and the maximum length of the fissures are decreasing with the increase in the confining pressure. In addition, the three-dimensional fractal dimension and the internal damage also decreased continuously with the increase in the confining pressure. This research provides valuable theoretical guidance for supporting and constructing surrounding rock in deep engineering projects.

Keywords: damaged rocks; dynamic properties; three-dimensional reconstruction; quantitative representation of fissure; three-dimensional fractal dimension



Citation: Chen, L.; Chu, H.; Wang, D.; Sun, B.; Wen, Z.; Wei, H. Quantitative Representation of Dynamic Mechanical Properties and Internal Damage in Deep-Seated Damaged Granite. *Appl. Sci.* **2024**, *14*, 10813. <https://doi.org/10.3390/app142310813>

Academic Editor: Giuseppe Lacidogna

Received: 29 October 2024
Revised: 20 November 2024
Accepted: 21 November 2024
Published: 22 November 2024



Copyright: © 2024 by the authors. Licensee MDPI, Basel, Switzerland. This article is an open access article distributed under the terms and conditions of the Creative Commons Attribution (CC BY) license (<https://creativecommons.org/licenses/by/4.0/>).

1. Introduction

With the continuous development of underground engineering construction, the development of China's underground resources is gradually deepening. Compared to shallow projects, deep underground projects are facing geological hazards, and engineering risks are more complex and variable [1], especially in the use of "drilling and blasting" construction, where the instantaneous strong impact load will bring about a more unpredictable risk of underground engineering. Due to the limitations of shallow rock mechanics, the existing relevant theories cannot be applied well to deep engineering [2]; based on this problem, scholars have carried out a lot of research.

In the construction of underground engineering, the surrounding rock is affected by construction disturbance and geological tectonic movement, resulting in there being different degrees of internal damage. Regarding the mechanical properties of damaged rock, Dai Bing et al. [3] conducted dynamic mechanical tests on granite with prefabricated parallel fissures and investigated the effects of prefabricated fissure angles and impact rates on energy dissipation and damage in granite. Liu et al. [4] prefabricated sandstones with different fissure angles, combined with digital image technology to carry out an impact test, revealing that increasing impact rates and crack angles enhanced the dynamic strength of sandstone and made crack propagation more complex. Yan et al. [5] used a split Hopkinson bar device to obtain dynamic mechanical properties, fracture characteristics, and energy evolution laws for sandstones with multiple parallel fissures. The results of

Wen Lei et al. [6] and Ping Qi et al. [7] showed that the original cracks in the rock affect the dynamic properties and crack extension of the rock. Niu et al. [8] used a crack propagation instrument to record the crack propagation parameters of the single-cleavage triangular sandstone sample under impact and calculated the dynamic stress intensity factor of the rock samples. Additionally, in deep environments, the influence of high crustal stress on the surrounding rock is not to be underestimated. Experiments using Hopkinson devices capable of applying a confining pressure are a common method of investigating such problems. In this regard, Du et al. [9] investigated the damage pattern of rocks using a split Hopkinson bar to which a confining pressure can be applied. You et al. [10] investigated the dynamic mechanical properties and energy dissipation law of fissured sandstones under different confining pressures. Yuan et al. [11] used cylinders of three different materials to achieve the pressurization of the rock and investigated the dynamic properties and damage modes of the rock. The above literature has carried out extensive studies on the dynamics of damaged rocks. But rock is a non-homogeneous natural material, and the development of internal pore fracture after perturbation is highly uncertain, and artificially prefabricated fissures do not reflect well the internal conditions of damaged rocks in actual engineering.

The change in the macroscopic mechanical properties of rock mass is caused by the change in the meso-mechanical properties and microscopic pore structure. To better study the microscopic changes in rocks, CT scanning technology has been introduced into the study of rock mass mechanics and has been widely used. Huang et al. [12] analyzed the mineral composition of rock based on CT scan images and determined the spatial distribution of each component in the rock sample based on three-dimensional reconstruction. Tan Wenhui et al. [13] carried out uniaxial compression tests and CT scans on jointed granite, studying the extension of internal joints. Liu et al. [14] reconstructed three-dimensional visualization fractures based on CT images and analyzed the relationship between the damage degree and the fractal dimension. Three-dimensional reconstruction based on CT scan images can provide a good understanding of the development and propagation of internal cracks in the loaded rock samples [15–17] and can quantitatively analyze the internal fissure [18]. Zhao et al. [19] used CT technology to define the damage ratio, integrity, and porosity of rock triaxial compression and studied the evolution process of two-dimensional and three-dimensional fractures based on two-dimensional images and three-dimensional models. Wang et al. [20] explored the rock crack propagation mode during cyclic loading and unloading by three-dimensional reconstruction, quantitatively describing the crack. Scholars have also conducted extensive exploratory research on methods for reconstructing three-dimensional models [21,22]. Although there are many methods for three-dimensional reconstruction, most of the results are still validated against analyses from Avizo software, indicating that Avizo has significant advantages in rock three-dimensional reconstruction [23,24].

There are many studies in the existing literature on rock dynamic properties and the three-dimensional reconstruction of rocks. However, there are very few studies that combine confining pressure, dynamic tests, and three-dimensional reconstruction techniques. In response to this issue, this paper takes granite as the research object and creates initial damage to the rock sample by impact. The dynamic mechanical properties of rocks with initial damage under different confining pressures are studied using the Hopkinson test. A group of impacted rock samples is selected for the CT test to analyze the influence of confining pressure on the evolution of internal fissures in the rock samples, and the quantitative representation of the fissure and rock sample three-dimensional fractal dimension are carried out. These research results can provide a certain theoretical reference for the support of surrounding rock in deep engineering.

2. Materials and Methods

2.1. Rock Sample Preparation

In this test, granite samples were obtained from a depth of one kilometer at a gold mine in Shandong, China. The authors' team has analyzed the mineral composition of the granite

used in this experiment in previous studies, and the results show that its main components are hornblende, feldspar, quartz, kaolinite, etc., with hornblende accounting for about 47.3% of the total composition, feldspar accounting for 40% of the total composition, quartz accounting for about 6.9% of the total composition, and kaolinite accounting for about 5.8% of the total composition [25]. The samples were prepared as cylindrical rock specimens with a diameter of 50 mm and a height of 25 mm, and they were uniform in texture, with no visible cracks, end face flatness ≤ 0.02 mm, and axial perpendicularity $\leq 0.25^\circ$.

The propagation speed of the sound wave as it passes through the rock will vary depending on the internal structural features. Therefore, the measurement results of wave velocity can be used as a reference material to judge the internal damage of rock samples. In this paper, the ZT801 geotechnical acoustic tester is used to measure the longitudinal wave velocity of the rock samples. Based on the basic theory of damage mechanics, the longitudinal wave velocity is defined as the damage variable, and the expression of this damage variable is shown in Equation (1) [26]:

$$S_n = 1 - \left(\frac{V_n}{V_0}\right)^2, \quad (1)$$

In the equation, S_n is the degree of damage; V_0 is the longitudinal wave velocity of the rock sample before impact, m/s; and V_n is the longitudinal wave velocity of the rock sample after impact, m/s.

To meet the test requirements, the rock samples were pre-treated as follows:

- (1) Ultrasonic Testing: The longitudinal wave velocities of the rock samples were measured using ultrasonic testing to exclude those with significant dispersion. The longitudinal wave velocity of the final stayed rock samples was mostly stabilized at 5680 m/s.
- (2) Initial Damage Creation: In preliminary tests, it was found that the critical impact air pressure for reaching a critical failure state under impact loading was 0.5 MPa. Two initial damage states were created with impact air pressures of 0.2 MPa and 0.3 MPa. The longitudinal wave velocity of the rock samples after 0.2 MPa and 0.3 MPa impacts was stabilized at 4810 m/s and 5260 m/s, respectively. Additionally, one set of rock samples was left undamaged. The damage levels of the three groups of rock samples were calculated as 0%, 14%, and 28%, respectively, according to Equation (1). Thus, there were three initial damage states: no damage, low damage, and moderate damage. Some rock samples are shown in Figure 1.



Figure 1. Some granite samples.

2.2. Dynamic Test Introduction

For the dynamic test, we used the Split Hopkinson Pressure Bar, which consists of a striker, an incident bar, a transmitted bar, an absorbed bar, a confining pressure device, and a data acquisition system. The total length of the incident bar is 2400 mm, the end in contact with the striker is a variable cross-section, the length of the variable cross-section is 170 mm, and the diameters of the two ends are 37 mm and 50 mm, respectively. The diameter of the striker is 37 mm, and the length is 400 mm. The length of the transmitted

bar is 1200 mm, and the diameter is 50 mm. The wave speed of the bars is 5190 m/s, the density is 7800 kg/m³, and Young's modulus is 210 GPa. The confining pressure device consists of an oil pumping device, a pressure chamber, and a pressure control system. When using the device, we first use the hot melt pipe to fix the rock samples in the pressure chamber and then fill the oil into the pressure chamber through the oil pumping device; when the pressure chamber is full of oil, we turn off the oil pumping device and then set the predetermined value of the pressure chamber on the pressure control system and click the button of pressurization, where the system will then be like a syringe squeezing the oil into the chamber to increase the pressure to the preset value. The Split Hopkinson Pressure Bar is shown in Figure 2.

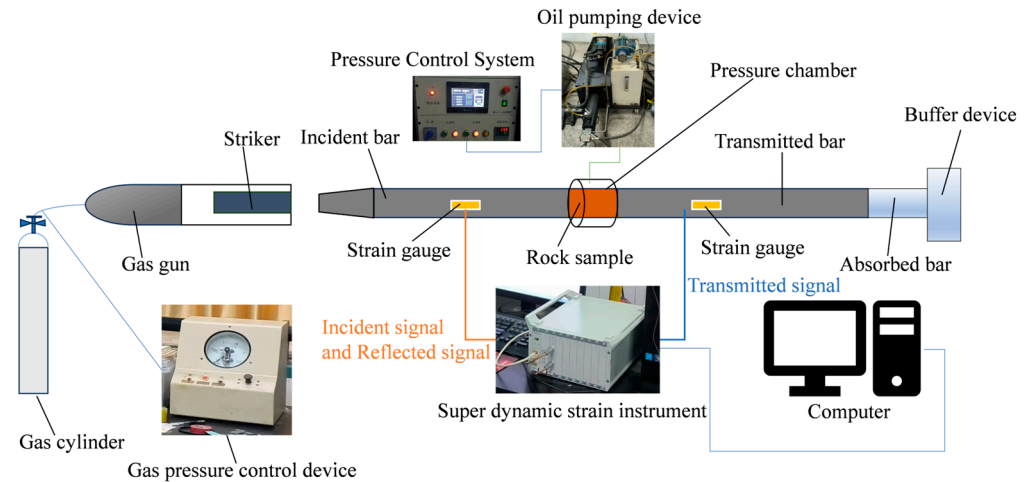


Figure 2. Schematic diagram of the Split Hopkinson Pressure Bar.

When using the Split Hopkinson Pressure Bar, the size of the impact air pressure is set on the gas pressure control device first and nitrogen gas is released when the value of the air pressure in the gas gun is added to the set value. The rapidly released gas produces a larger pressure to drive the bullet to hit the incident bar to produce a shock wave to be transmitted to the rock samples, which are deformed at high speed under the impact loading. The whole process is recorded as a pulse signal by strain gauges and collected by the DH8302 dynamic signal test system designed by Donghua Company. The dynamic stress and strain parameters of the rock samples are analyzed by the supporting computer software.

The Hopkinson test satisfies two basic assumptions:

One-dimensional elastic stress wave assumption: the propagation path of the stress wave in the Hopkinson bar is one-dimensional, and the stress wave in any cross-section in the bar is in the same horizontal plane. That is, the axial strain measured at the surface of the compression bar can represent the axial strain of the entire cross-section. Stress-strain uniformity assumption: that is, the stress and strain of the rock sample in the length direction are uniform.

Based on the above two assumptions, the equation for the average stress $\sigma(t)$, average strain $\varepsilon(t)$, and average strain rate $\dot{\varepsilon}(t)$ of the specimen can be obtained [27,28]:

$$\sigma(t) = \frac{A_e}{2A_s} E_s [\varepsilon_I(t) - \varepsilon_R(t) - \varepsilon_T(t)], \quad (2)$$

$$\varepsilon(t) = \frac{C_s}{L} \int_0^t [\varepsilon_I(t) - \varepsilon_R(t) - \varepsilon_T(t)] dt, \quad (3)$$

$$\dot{\varepsilon}(t) = \frac{C_s}{L} [\dot{\varepsilon}_I(t) - \dot{\varepsilon}_R(t) - \dot{\varepsilon}_T(t)], \quad (4)$$

where A_e and A_s are the cross-sectional area of the incident bar and sample, mm². E_s is the modulus of elasticity of the incident bar, GPa. $\varepsilon_I(t)$, $\varepsilon_R(t)$, and $\varepsilon_T(t)$ are the strain signals

of incident wave, reflected wave, and transmitted wave at the moment of t , respectively. C_s is the longitudinal wave speed of the incident bar, m/s. L is the length of the sample.

Based on the above rationale, a pre-experiment was carried out. The strain signals obtained after impact were analyzed, as shown in Figure 3. The waveform is generally smooth, and no dispersion effects are observed during the propagation of the stress waves. The sum of the incident and reflected waves' amplitudes is nearly consistent with the amplitude of the transmitted wave, indicating that the rock sample was in dynamic stress equilibrium before impact failure. This test result establishes the foundation for the accuracy of the experimental data. It is also worth noting that there was no confining pressure applied for this test.

The dynamic test plan is as follows: The initial damage state is categorized into three groups (no damage, low damage, and moderate damage), and four confining pressure levels (5 MPa, 10 MPa, 15 MPa, 20 MPa) are set for each group. The impact air pressure is kept constant at 0.5 MPa during each test. To ensure data accuracy, each condition is tested three times, and the results are averaged from the three tests. In addition, the dynamic properties of these three damage state rock samples without confining pressure have been described by the author team in a previously published paper [25]. The obtained stress–strain curves are shown in Figure 4, so this is not repeated in this paper.

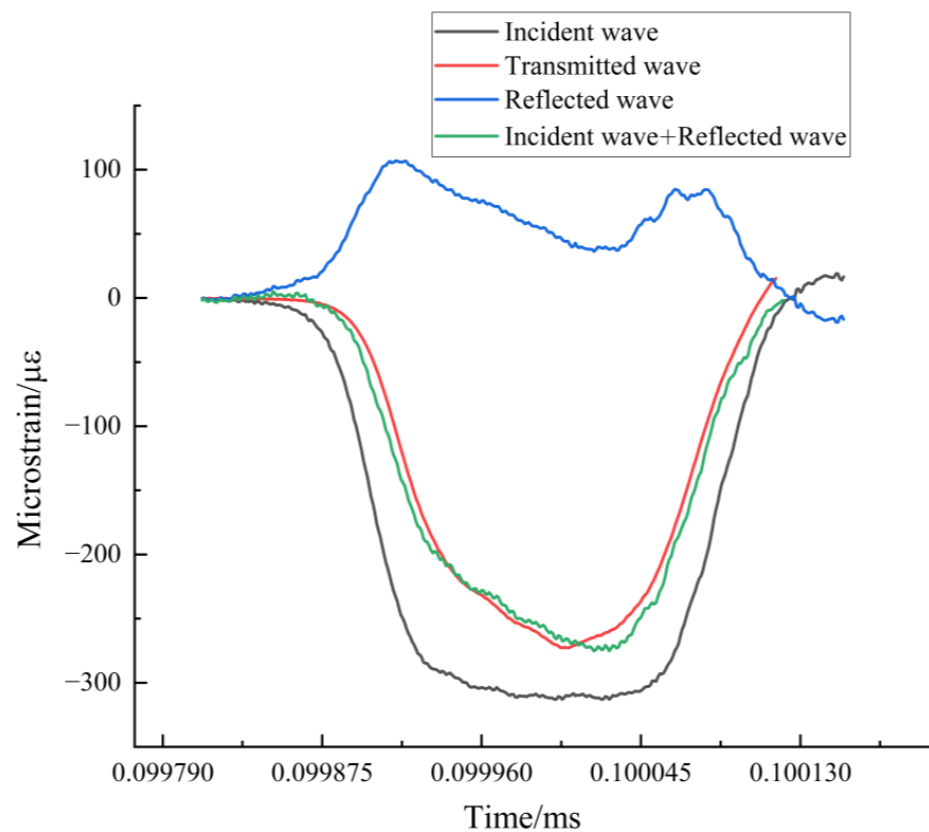


Figure 3. Dynamic stress balance verification.

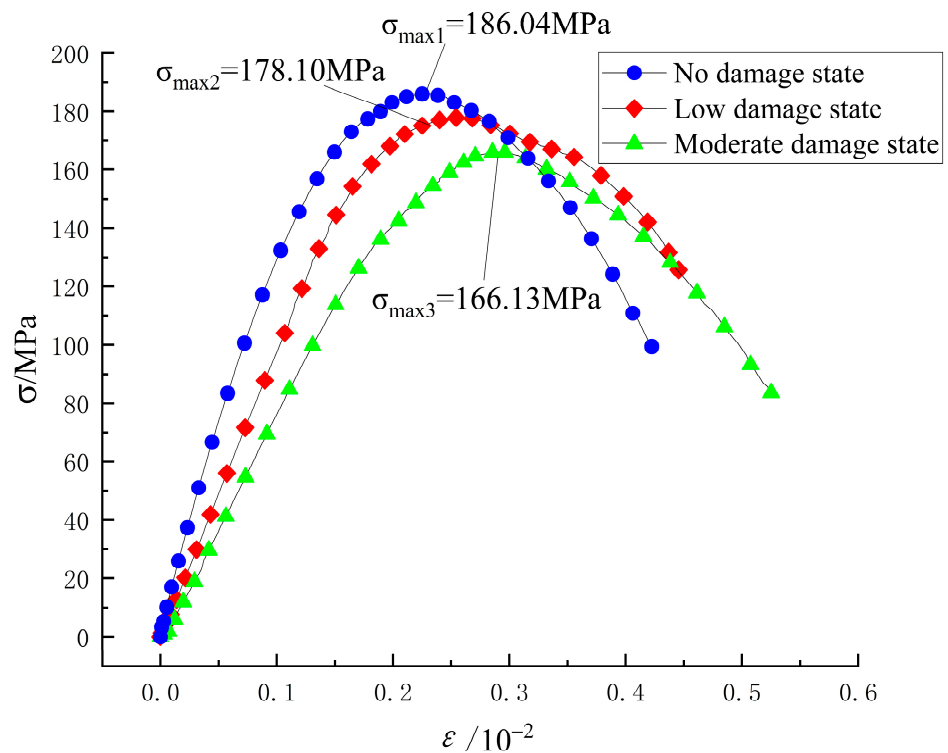


Figure 4. Stress–strain curves of rock samples in three states of damage without confining pressure.

2.3. CT Scan Test

The CT test uses a coal and rock industrial CT scanning system (Phoenix v | tome | x s) with load capacity. The device can perform continuous high-precision three-dimensional CT scanning of coal and rock samples under non-loading conditions. The maximum diameter for a complete scan is 230 mm, with a height of 420 mm. The device is equipped with two X-ray tubes: one is a high-power micro-focus X-ray source with a maximum tube voltage of 240 kV, a minimum focal spot size of $\leq 3 \mu\text{m}$, a maximum power of $\geq 320 \text{ W}$, and a detail resolution of $\leq 2 \mu\text{m}$; the other is a high-precision nano-focus X-ray source with a maximum tube voltage of 180 kV, a minimum focal spot size of $\leq 1 \mu\text{m}$, maximum power of $\geq 15 \text{ W}$, and a detail resolution of $\leq 0.5 \mu\text{m}$. This device can scan internal pores, damage, and other features of the samples, providing data for subsequent three-dimensional reconstruction. The CT test plan is as follows: select untreated rock samples and a group of rock samples with an initial state of no damage, which have been impacted under different confining pressures, for scanning.

2.4. Three-Dimensional Reconstruction Methods

The information obtained from the two-dimensional CT images of the rock samples is quite limited and only allows for a basic qualitative analysis. Avizo 2020.1 software is a professional 3D visualization modeling software. It is capable of completing 3D visualization modeling based on CT images. The software provides a large number of data types and modules to quickly complete the quantitative analysis of 3D model data. This paper mainly applies the ortho slice command, interactive thresholding command, volume rendering command, label analysis command, and fractal dimension command in Avizo 2020.1. These commands are used to extract the fracture of rock samples, reconstruct the fracture in three dimensions, count the fracture parameters, and calculate the three-dimensional fractal dimension. The reconstruction process is illustrated in Figure 5.

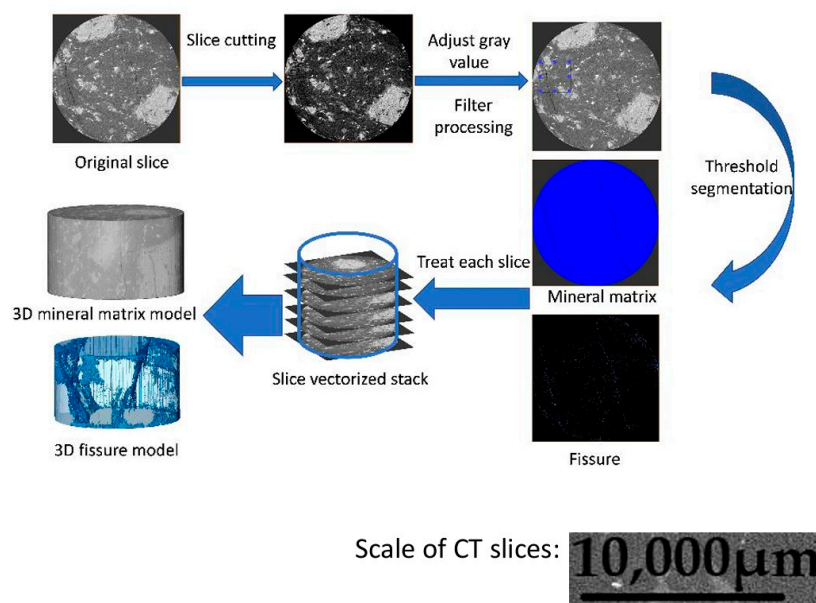


Figure 5. Flowchart of 3D model reconstruction.

The three-dimensional reconstruction process using Avizo 2020.1 software involves the following steps:

- (1) **Importing Images:** First, the images obtained from the CT scan are imported into the software. Since the tape used to wrap the samples during scanning can introduce artifacts, the images are cropped to remove these artifacts and minimize their impact on the results.
- (2) **Noise Reduction:** Due to external noise during scanning, the original images may contain noise. To enhance image quality for subsequent analysis, the grayscale values are adjusted, and filtering is applied to reduce noise.
- (3) **Threshold Segmentation:** Accurate segmentation of different phases in the image is crucial for three-dimensional reconstruction. Common algorithms for threshold segmentation include watershed segmentation, global thresholding, and region growing. In this study, Avizo 2020.1 software's built-in watershed algorithm is used, which is effective in accurately identifying voxels at the boundaries where different phases intersect. Additionally, there is a linear relationship between the grayscale value and the density of mineral components: higher brightness indicates higher density. In the scanned two-dimensional images, brighter regions correspond to mineral components (such as amphibole, feldspar, quartz, etc.), while darker regions indicate fissures. During processing, the grayscale values are used to differentiate between fissures and mineral matrix.
- (4) **Three-Dimensional Rendering:** After threshold segmentation, the original images are classified into two phases (mineral matrix and fissures). The software then renders and visualizes the rock samples in three dimensions, showcasing the internal structure and features.

3. Results

3.1. Results of the Hopkinson Test

The data measured by Hopkinson's test are shown in Table 1, and the stress–strain curve is shown in Figure 6.

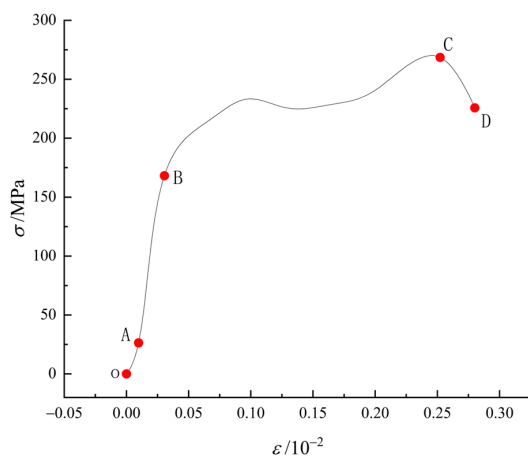
From Table 1, it can be seen that when the initial damage state of the rock samples is certain, both the strain rate and the peak stress keep increasing with the increase in the confining pressure. When the rock samples are in the no-damage state, the change in strain rate is the largest, increasing from 153 s^{-1} to 188 s^{-1} . The increase in the confining pressure also increases the peak stress of the rock samples. However, the effect of initial damage on

the strain rate and peak stress was opposite, and a decrease in both the strain rate and peak stress occurred with increasing damage.

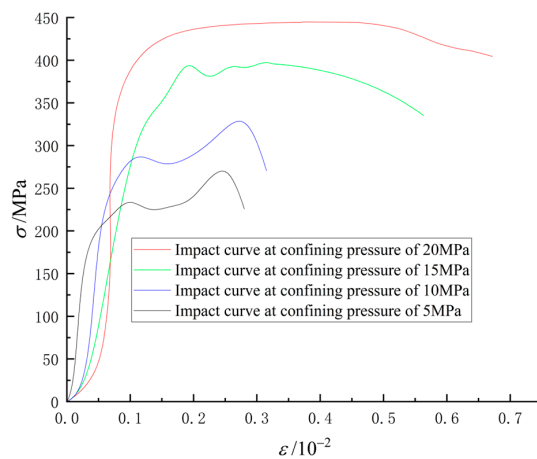
The stress–strain curve under no damage and confining pressure of 5 MPa is taken as a typical stress–strain curve for analysis, as shown in Figure 6a. The stress–strain curve can be roughly divided into four stages: compaction stage (OA segment), elastic deformation stage (AB segment), plastic deformation stage (BC segment), and post-peak stage (CD segment).

Table 1. Test results of granite under different states.

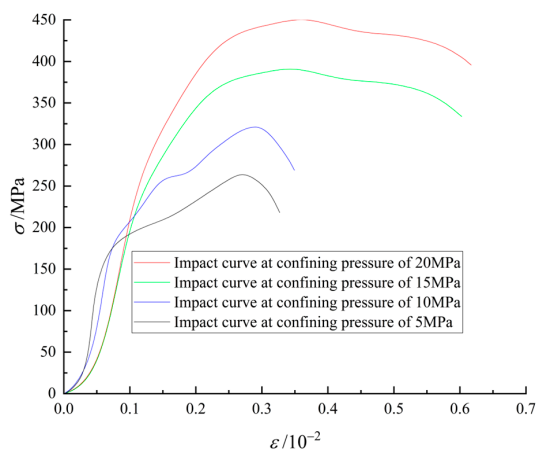
Damage Degree	Impact Air Pressure	Confining Pressure/MPa	Average Strain Rate /s ⁻¹	Peak Stress /MPa
No damage		5	153	270.10
		10	165	328.49
		15	173	397.13
		20	188	450.12
Low damage	0.5 MPa	5	150	263.67
		10	164	321.01
		15	165	390.77
		20	176	447.45
Moderate damage		5	152	250.72
		10	160	309.78
		15	167	382.87
		20	170	444.72



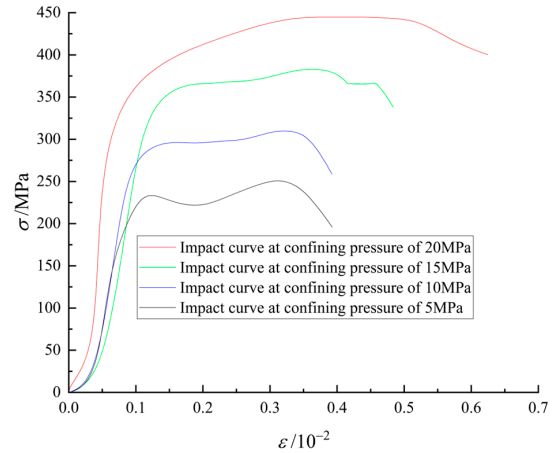
(a) Typical stress–strain curves



(b) Stress–strain curves of no damage granite under different confining pressures



(c) Stress–strain curves of low damage granite under different confining pressures



(d) Stress–strain curves of moderate damage granite under different confining pressures

Figure 6. Stress–strain curves of granite under different states.

Compaction stage (OA segment): From the stress–strain curve, the slope of the curve in this stage is smaller than that of the elastic stage. During this stage, the minor fissures and cracks within the rock sample are compacted [29]. As confining pressure increases, this stage becomes more pronounced. But the initial damage has the opposite effect. The reason for this is that the increase in initial damage leads to an increase in the number of fissures in the rock sample, which causes changes that delay the microcracks from closing before the impact load begins to develop, and the sample directly enters the next stage, showing a decrease in peak stress in mechanical properties.

Elastic deformation stage (AB segment): In this stage, the stress–strain curve is close to a straight line, and the slope can be used as the dynamic elastic modulus of the rock sample. After the compaction stage, the internal components of the rock sample are in more thorough contact, and the sample undergoes elastic deformation under load. It can be seen from Figure 6b–d that the slope of this stage increases with the increase in confining pressure, while the duration of the elastic deformation stage decreases.

Plastic deformation stage (BC segment): After entering this stage, the tangent slope of the stress–strain curve decreases continuously, and the stress exhibits certain fluctuations and reaches a peak. The reason for this is that the independent pores and microcracks in the rock sample begin to expand first; when they expand to a certain extent, relatively independent pores and microcracks gradually connect to form larger interconnected fissures. When the confining pressure increases to 15 MPa, the stress–strain curve in this stage shows a smoother trend. The existence of confining pressure makes the development of microcracks in rock samples more stable.

Post-peak stage (CD segment): As the deformation continues, the stress of the rock sample gradually declines after reaching its peak. Although strain continues to increase, the rate of increase becomes progressively smaller. This indicates that a few microcracks within the rock sample are still expanding during this stage. The increase in confining pressure will increase the maximum strain value of the rock sample.

3.2. Results of CT Scan

Due to the use of critical air pressure for the impact tests in this experiment, the granite samples did not produce a large number of fragments under the combined effects of confining pressure and impact load. To better understand the changes in the internal fissure of the rock samples after impact, a set of no-damaged rock samples was selected. These samples were subjected to impact testing under different confining pressures and then underwent industrial CT scanning. Three-dimensional reconstruction techniques were applied to process the scanned CT images, and the reconstructed 3D models were analyzed to examine the internal changes.

During the CT scanning process, each test rock sample was scanned to produce 1000 slices, with the first slice corresponding to the end of the sample subjected to the incidence bar, and the slices numbered sequentially. The CT scan results of both the untreated rock samples and a group of no-damage samples to impact load under different confining pressures are shown in Figure 7.

Figure 7a shows that granite, being a dense rock, contains very few large pores or microcracks internally. In particular, the rock samples used in this experiment were extracted from depths of several kilometers, where years of evolution have resulted in very few microscopic pores, indicating that the selected samples are highly suitable for testing.

We compared the CT scan images of the group of no-damage rock samples subjected to impacts under different confining pressures (Figure 7). It is evident that as confining pressure increases, the number, width, and complexity of fissure in the transverse slices of the rock samples decrease. This phenomenon is also clearly observed in the front views of the rock samples. The underlying reason for this is that under impact loads, the confining pressure restricts the transverse deformation of the rock, thereby impeding the expansion of the internal fissure. This effect becomes more pronounced with increasing confining pressure. Additionally, the presence of confining pressure alters the failure mode of the

rock. At low confining pressures, the rock primarily experiences tensile–shear mixed failure. However, as confining pressure increases, the failure mode shifts to purely shear failure, a transition that is particularly evident in the front views of the CT images shown in Figure 7.

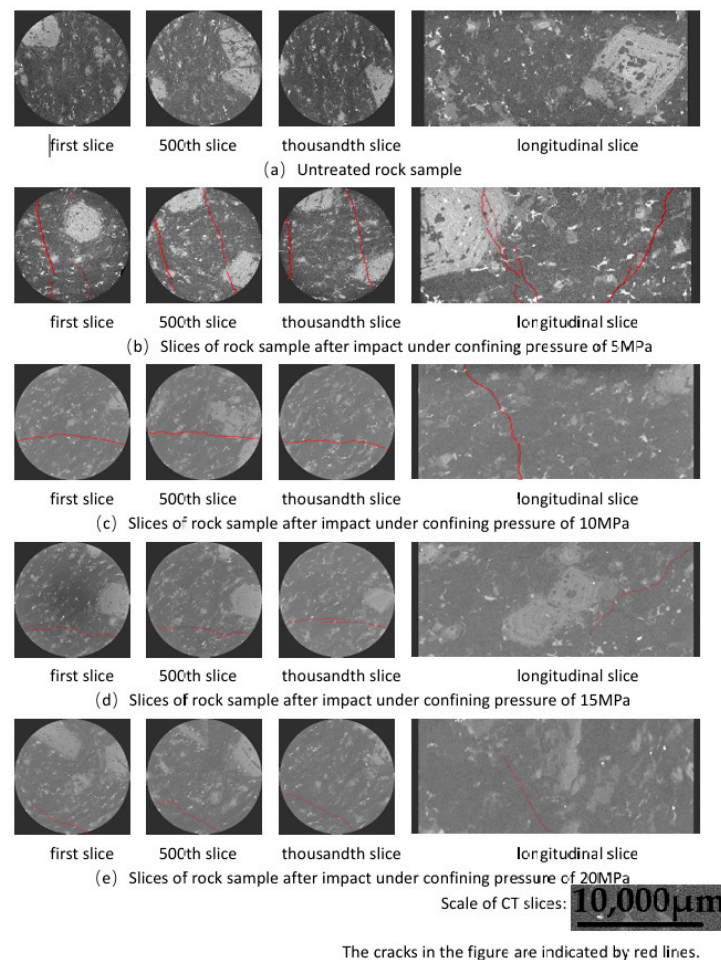


Figure 7. CT scan slices of rock samples in different states.

4. Discussions

4.1. Analysis of Dynamic Parameters

In order to better evaluate the dynamic characteristics of granite, the results of three parameters, peak stress, peak strain, and peak modulus, are selected in this paper.

To specifically analyze the extent to which confining pressure and initial damage affect the dynamic mechanical properties of granite samples, the peak stress of 270.10 MPa for no-damaged rock samples under a confining pressure of 5 MPa is used as a reference. The damage-weakening factor f_s is introduced for calculation and analysis, with its calculation given by Equation (5) [30]:

$$f_s = \left(\frac{\sigma_n - \sigma_1}{\sigma_1} \right) \times 100\%, \quad (5)$$

In the equation, σ_n is the peak stress of granite samples under different states, and σ_1 is the peak stress of no-damaged rock samples under a confining pressure of 5 MPa. If f_s is positive, this means that the peak stress of the rock sample has increased compared to σ_1 ; otherwise, it means a decrease. The f_s calculation results of the weakening coefficient of granite rock samples in different states are shown in Table 2.

Table 2. Influence degree of initial damage and confining pressure on peak stress of granite samples.

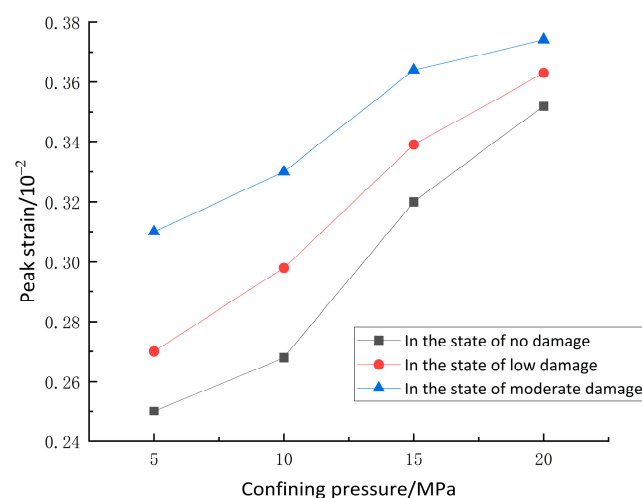
Damage Degree	Confining Pressure			
	5 MPa	10 MPa	15 MPa	20 MPa
No damage	0.00%	21.62%	47.03%	66.65%
Low damage	−2.38%	18.85%	44.68%	65.66%
Moderate damage	−7.17%	14.69%	41.75%	64.65%

It can be seen from Table 2 that the peak stress of granite samples under different confining pressures decreases continuously with the increase in initial damage, and the peak stress of rock samples with different initial damage increases continuously with the increase in confining pressure. The increase in confining pressure will reduce the impact of initial damage on the peak stress, which is particularly obvious at a confining pressure of 20 MPa. The analysis of the internal reasons shows that the initial damage leads to the increase in porosity inside the rock sample, especially the increase in the connectivity between the pores and fissures, which leads to the acceleration of the penetration of the pores and fissures and the decrease in the bearing capacity of the rock sample under the impact load. When confining pressure is applied, the micropores inside the rock sample are closed, and the void between the matrix of the rock sample is reduced. With increasing confining pressure, the pore cracks caused by the initial damage will be further compacted until they are completely closed, which is reflected in the increase in peak stress in the dynamic characteristics of the rock.

To analyze the effects of confining pressure and initial damage on the deformation of granite samples under impact load, this paper selected peak strain and peak modulus as the analysis objects. Peak strain is the strain value corresponding to the peak stress in the stress–strain curve of a rock, and peak modulus is the ratio of peak stress to peak strain. Compared with the modulus of elasticity, the peak modulus expresses the rock's ability to resist deformation at various stages under impact loading [31].

The relationships between the peak strain and peak modulus of rock samples and the confining pressure under different states are shown in Figures 8 and 9.

As illustrated in Figure 8, confining pressure and initial damage have varying impacts on the peak strain of granite samples under impact load. Specifically, at the same confining pressure, an increase in initial damage leads to a higher peak strain in the samples. Additionally, for samples with the same initial damage state, peak strain increases with higher confining pressure. However, this promoting effect of confining pressure on peak strain diminishes as confining pressure continues to rise.

**Figure 8.** Peak strain of rock samples after impact in different states.

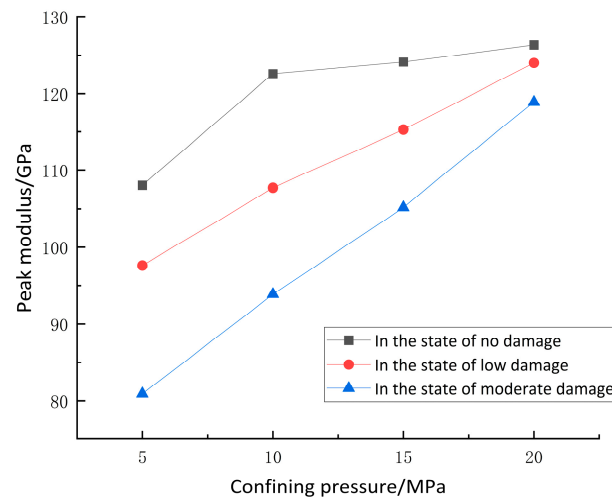


Figure 9. Peak modulus of rock samples after impact in different states.

This behavior can be explained by the fact that initial damage increases the porosity within the samples, introducing irreversible deformation. Under impact load, this deformation is further exacerbated. While confining pressure enhances the sample's ability to resist elastic deformation, once the deformation exceeds the elastic limit of the sample, confining pressure becomes a force that exacerbates deformation. This is manifested by the further expansion of internal cracks and increased deformation. Nevertheless, this effect weakens with higher confining pressure because increased confining pressure enhances the sample's resistance to elastic deformation.

The peak modulus effectively reflects the deformation characteristics of rock samples under impact loads at various stages, particularly its ability to resist deformation. It is defined as the ratio of peak stress to peak strain. As shown in Figure 9, under the same confining pressure, the peak modulus of the rock samples decreases with increasing initial damage, indicating that initial damage reduces the rock's ability to resist deformation. Under the same initial damage state, the peak modulus of the rock samples increases with higher confining pressure. Compared to low confining pressures, the influence of initial damage on the peak modulus is less significant at high confining pressures, with confining pressure having a more dominant effect. The underlying reason is that increased confining pressure leads to the further closure of microcracks caused by initial damage, making the rock sample denser and thus increasing its peak modulus.

4.2. Quantitative Fracture Analysis

To conduct a more detailed quantitative analysis of the changes in internal fissures of the group of no-damaged rock samples subjected to impact loads under different confining pressures, three-dimensional reconstruction of the two-dimensional CT images was performed using Avizo 2020.1 software.

The three-dimensional reconstruction models of the group of no-damaged granite rock samples subjected to impact under different confining pressures are shown in Figure 10.

From the three-dimensional reconstruction models of rock samples under different conditions shown in Figure 10, the impact of confining pressure on the development of fissures in the rock samples is evident. For the untreated rock samples, there are only a few isolated, small-volume pores with limited connectivity. After impact, numerous through fissures develop, which are the primary cause of the rock's fracturing. As confining pressure increases, the number of through fissures decreases. Particularly, when the confining pressure reaches 15 MPa, the number of through fissures within the rock samples is notably reduced, and at 20 MPa, no large-volume fissures are observed.

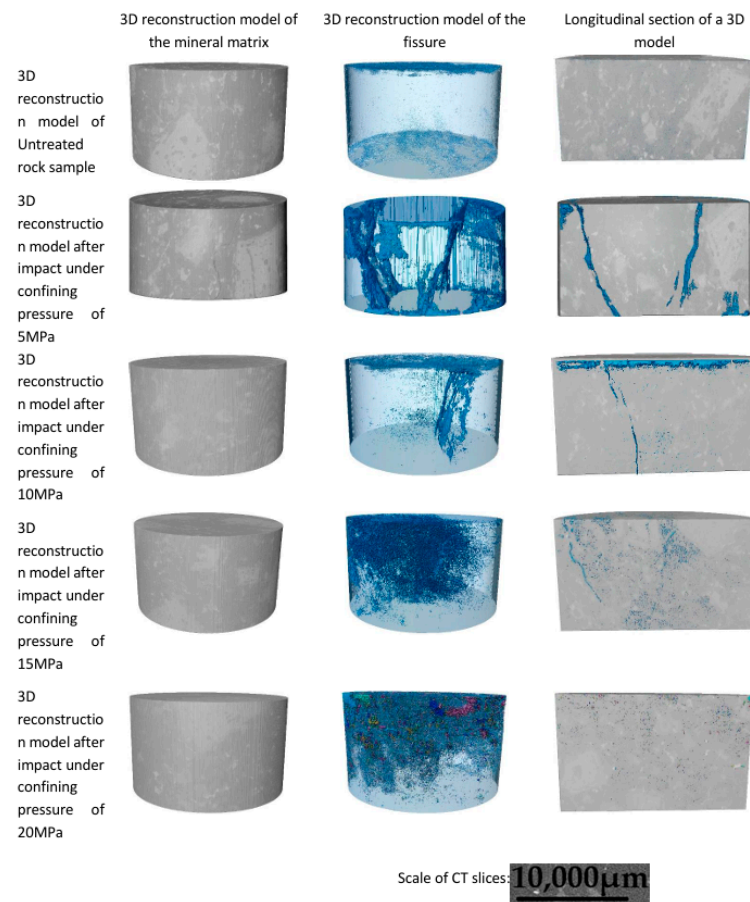


Figure 10. Three-dimensional reconstruction models of rock samples under different states.

Under impact loading, the influence of confining pressure on the internal development of fissures is more clearly depicted in the three-dimensional reconstruction models. From the longitudinal section of the rock sample in Figure 10, the evolution law of the pore fracture can be observed. As discussed in the analysis of granite dynamic deformation, impact loading causes axial deformation in the rock sample, and due to the Poisson effect, transverse deformation also occurs. However, the presence of confining pressure restricts transverse deformation and alters the development direction of the fissures, causing them to gradually shift towards the center of the rock sample. The specific impact of confining pressure on fissures' development is illustrated in Figure 11. Increased confining pressure makes the internal through fissures of the rock sample more linear, with this effect being particularly pronounced at 10 MPa.

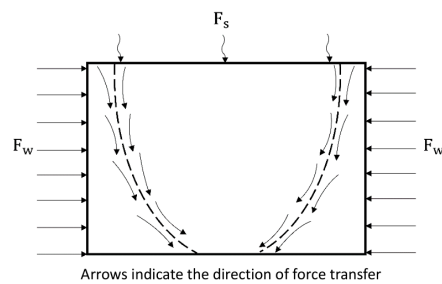


Figure 11. Schematic diagram of the influence of confining pressure on impact fissure development. Note: F_s is impact load; F_w is confining pressure force.

The primary cause of rock failure is the propagation and development of internal fissures. Quantitative analysis of these fissures using the three-dimensional reconstruction

models of the rock samples provides a fundamental explanation of how confining pressure affects the macroscopic mechanical properties of granite samples after impact. In this analysis, the internal fissures of the rock samples are categorized into fissures and independent fissures. The main cause of rock failure is the formation of through fissures that connect and penetrate the rock sample under external forces, while the remaining fissures that do not penetrate the rock are considered independent fissures. The volume of fissures and the maximum length of through fissures are selected as parameters for quantitative analysis. The detailed analysis results are presented in Table 3.

Table 3. Statistical change in parameters of rock samples in different states after impact.

Sample State	Total Fissure Volume (nm ³)	The Volume Proportion of Through Fissure (%)	The Volume Proportion of Independent Fissure (%)	Maximum Through Fissure Length (nm)
After impact at a confining pressure of 5 MPa	39,474,100	95%	5%	76,101,952
After impact at a confining pressure of 10 MPa	7,961,934	73%	27%	54,654,324
After impact at a confining pressure of 15 MPa	4,052,681	32%	68%	51,974,100
After impact at a confining pressure of 20 MPa	2,947,010	17%	83%	36,900,516

From Table 3, it is observed that as confining pressure increases, the total volume of internal fissures in the rock samples decreases after impact. Specifically, the proportion of the volume occupied by through fissures decreases, while the proportion occupied by independent fissures increases. Additionally, the maximum length of through fissures also diminishes. These quantitative analysis results demonstrate the suppressive effect of confining pressure on the development of internal fissures in the rock samples. They also validate the qualitative findings of the impact of confining pressure on fissures discussed earlier and reveal the underlying reasons for the influence of confining pressure on the dynamic mechanical properties of the rock samples from the perspective of three-dimensional fissure evolution.

4.3. Three-Dimensional Fractal Dimension and Damage Analysis of Internal Fractures in Rock Samples

The fractal dimension, as a geometric method for describing the complexity of objects, can be used to quantitatively characterize the complexity of internal fissures in rock samples [32]. The principle for calculating the fractal dimension in Avizo 2020.1 software is as follows:

For an object with fractal characteristics, divide it into n equal units. The number of units, unit scale, and the number of units at different scales have relationships as described by Equation (6) [33]:

$$N(\delta) = \delta^{-D}, \quad (6)$$

where δ represents the smallest scale after dividing the object n times; $N(\delta)$ is the total number of units at the smallest scale δ ; and D is the fractal dimension, which corresponds to the number of units at different scales.

For the area A of the remaining fractal body after division, it is equal to the product of the area at the unit scale and the number of units at that scale, as given by Equation (7):

$$A = N(\delta) \cdot \delta^2, \quad (7)$$

By substituting Equation (6) into Equation (7), we obtain Equation (8):

$$A = \delta^{2-D}, \quad (8)$$

Equation (8) illustrates the relationship between the smallest scale δ , fractal area A , and fractal dimension D . Therefore, D represents the area fractal dimension. Extending this equation to three-dimensional space yields Equation (9):

$$V = \delta^{3-D_v}, \tag{9}$$

In Equation (9), V denotes the three-dimensional volume, and D_v is the three-dimensional fractal dimension.

In Euclid’s geometry, straight lines and curves are one-dimensional, planes and spheres are two-dimensional, and forms whose length, width, and height all exist are three-dimensional. But for complex forms, their dimensions are not described by integers like one, two, or three. This problem was solved by the advent of the Koch curve and the Menge sponge. The Koch curve occupies a limited area with its unlimited length, which is bigger than one dimension and smaller than two, i.e., its dimension is bigger than one and smaller than two. The Menge sponge is similar in principle; the surface area of the hole inside the Menge sponge is unlimited, but it occupies a limited three-dimensional space, so its dimension is between two and three [34]. From the above analysis, it is known that the three-dimensional fractal dimension is between two and three, a higher fractal dimension indicates greater complexity in the rock’s fissures, while a lower dimension suggests simpler fissure structures.

The use of fractal dimensions to analyze the extent of damage within a rock sample is a common method based on Yang’s definition [35] of damage:

$$w = \frac{D_v - D_0}{D_v^{max} - D_0}, \tag{10}$$

In Equation (10), w is the degree of damage; D_v is the fractal dimension of the rock sample after impact; D_0 is the fractal dimension of the rock sample before impact; and D_v^{max} is the maximum value of the fractal dimension of the rock sample after impact for the three-dimensional problem $D_v^{max} = 3$.

Based on the above principle, the authors have calculated the internal damage degree and three-dimensional fractal dimension of the rock samples under different circumferential pressures. And in connection with the damage-weakening factor in Section 4.1, Figure 12 was drawn.

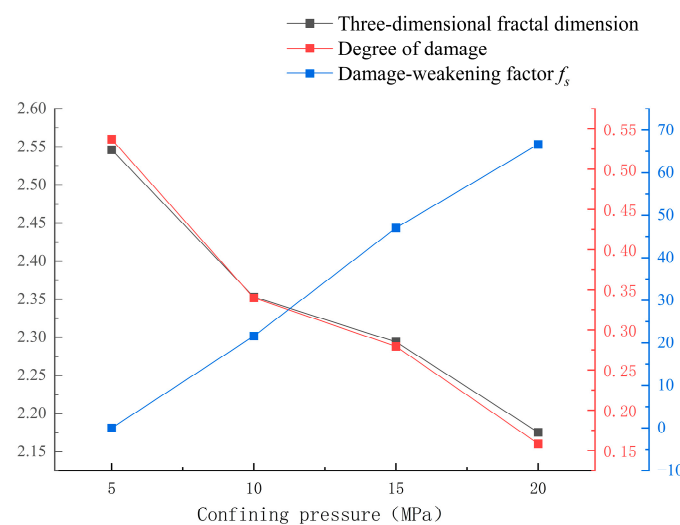


Figure 12. Relationship between internal damage, damage-weakening factor, and confining pressures.

From Figure 12, it can be seen that the three-dimensional fractal dimension of the rock samples after impact shows a gradual decrease with the increase in the confining pressure, and the reasons for this are analyzed as follows: under the low confining pressure, the

number of cracks inside the rock samples increases due to the impact, and the development and evolution of the cracks are very uncertain, resulting in the complexity of the cracks inside the rock samples, and the values of the three-dimensional fractal dimensions are larger. With the increase in the confining pressure, the development of the micropore cracks and the overall deformation of the samples are restricted, thus reducing the number and complexity of the pore cracks, resulting in a decrease in the values of the three-dimensional fractal dimensions. With the increase in the confining pressure, the development of microporous cracks and the overall deformation of the rock samples are restricted, and the number and complexity of the cracks are reduced, which leads to the decrease in the value of the three-dimensional fractal dimension of the rock samples. Secondly, the change amplitude of the three-dimensional fractal dimension and damage degree also slowed down with the increase in the confining pressure, the change amplitude of the three-dimensional fractal dimension decreased from 0.1933 to 0.1185, and the damage degree decreased from 0.1972 to 0.1209. The results, from the perspective of three-dimensional fractal dimensions, quantitatively examine the extent of the impact of confining pressure on the development of internal fissures in rock samples after impact, and this is consistent with the results of the quantitative crack analysis. Meanwhile, it can be seen from Figure 12 that the increase in confining pressure not only reduces the degree of damage inside the rock samples but also improves the impact resistance of the rock samples.

In this paper, dynamic tests on damaged rocks were carried out using a split Hopkinson bar, which can apply a confining pressure. The damage inside the rock samples after impact at different confining pressures was analyzed using three-dimensional reconstruction techniques. These results deepen our understanding of the dynamic properties and internal damage evolution of deeply damaged rocks.

5. Conclusions

1. The peak stress and peak modulus of the granite samples decrease gradually with increasing initial damage, while the peak strain increases with the initial damage. Under the same initial damage, all three parameters increase with rising confining pressure.
2. Confining pressure alters the evolution of internal fissures in granite samples. As confining pressure increases, the number and complexity of fissures in transverse sections decrease, and in longitudinal images, cracks within the rock sample shift progressively toward the center and become more linear.
3. With increasing confining pressure, the total volume of fissures gradually decreases. The proportion of the volume occupied by through fissures drops from 95% to 17%, and their maximum length reduces from 76,101,952 nm to 36,900,516 nm. Conversely, the proportion of the volume occupied by independent fissures increases from 5% to 83%. Additionally, the three-dimensional fractal dimension also decreases with increasing confining pressure, indicating that confining pressure reduces the internal damage in the rock samples.

Author Contributions: Conceptualization: L.C. and H.C.; methodology: D.W. and L.C.; validation: D.W., B.S., Z.W. and H.W.; writing—original draft preparation: D.W.; writing—review and editing: L.C.; supervision: H.W.; funding acquisition: H.C. All authors have read and agreed to the published version of the manuscript.

Funding: The authors thank the National Key Research and Development Program of China: Scaling-intelligent rock drilling and blasting technology and equipment for high-stress metal mines (No. 2023YFC2907202) and the National Natural Science Foundation of China: Basic research on continuous intelligent safe mining of deep metal mine (N0.52130403) for funding this study.

Institutional Review Board Statement: Not applicable.

Informed Consent Statement: Not applicable.

Data Availability Statement: The data that support the findings of this study are available from the corresponding author, Donghui Wang, upon reasonable request.

Acknowledgments: We would like to thank the Impact Dynamics Laboratory of the School of Civil Engineering, Henan University of Science and Technology, for facilitating this test.

Conflicts of Interest: Author Donghui Wang was employed by The Second Company of China Construction Second Engrg Bureau Ltd. The remaining authors declare that the research was conducted in the absence of any commercial or financial relationships that could be construed as a potential conflict of interest.

References

1. He, M.; Wu, Y.; Gao, Y.; Tao, Z. Research progress of rock mechanics in deep mining. *J. China Coal Soc.* **2024**, *49*, 75–99. [[CrossRef](#)]
2. Xie, H.; Zhang, R.; Zhang, Z.; Gao, M.; Li, C.; He, Z.; Li, C.; Liu, T. Reflections and explorations on deep earth science and deep earth engineering technology. *J. China Coal Soc.* **2023**, *48*, 3959–3978. [[CrossRef](#)]
3. Dai, B.; Zhao, G.; Zhang, L.; Zhang, Z.; Liu, Y.; Chen, Y. Experimental study of rock with parallel cracks under different loading rates: Energy dissipation and damage evolution. *Chin. J. Rock Mech. Eng.* **2024**, *43*, 3397–3412. [[CrossRef](#)]
4. Liu, L.; Li, H.; Zhang, G.; Fu, S. Dynamic strength and full-field cracking behaviors of pre-cracked rocks under impact loads. *Int. J. Mech. Sci.* **2024**, *268*, 109049, ISSN 0020-7403. [[CrossRef](#)]
5. Yan, Z.; Dai, F.; Liu, Y.; Du, H. Experimental investigations of the dynamic mechanical properties and fracturing behavior of cracked rocks under dynamic loading. *Bull. Eng. Geol. Environ.* **2020**, *79*, 5535–5552. [[CrossRef](#)]
6. Wen, L.; Feng, W.; Li, M.; Kou, Z.; Wang, L.; Yu, J. Strain rate effect on crack propagation and fragmentation characteristics of red sandstone containing pre-cracks. *Explos. Shock Waves* **2023**, *43*, 113103. [[CrossRef](#)]
7. Ping, Q.; Sun, S.; Gao, Q.; Wu Sh Li, X.; Xu, Y.; Hu, J.; Tang, Q. Study on dynamic mechanical properties and crack extension law of water-saturated fractured sandstone. *Chin. J. Rock Mech. Eng.* **2024**, *43*, 3131–3139. [[CrossRef](#)]
8. Niu, C.; Zhu, Z.; Deng, S.; Ying, P.; Qiu, H.; Wang, F.; Zhou, L. Effect of Loading Rate and Water on the Dynamic Fracture Behavior of Sandstone under Impact Loadings. *Int. J. Geomech.* **2021**, *21*, 04021139. [[CrossRef](#)]
9. Du, H.-B.; Dai, F.; Xu, Y.; Yan, Z.; Wei, M.-D. Mechanical responses and failure mechanism of hydrostatically pressurized rocks under combined compression-shear impacting. *Int. J. Mech. Sci.* **2020**, *165*, 105219, ISSN 0020-7403. [[CrossRef](#)]
10. You, W.; Dai, F.; Liu, Y.; Yan, Z. Effect of Confining Pressure and Strain Rate on Mechanical Behaviors and Failure Characteristics of Sandstone Containing a Pre-existing Flaw. *Rock Mech. Rock Eng.* **2022**, *55*, 2091–2109. [[CrossRef](#)]
11. Yuan, F.; Prakash, V.; Tullis, T. Origin of pulverized rocks during earthquake fault rupture. *J. Geophys. Res.* **2011**, *116*, B06309. [[CrossRef](#)]
12. Huang, C.; Zhang, X.; Liu, S.; Li, N.; Kang, J.; Xiong, G. Construction of pore structure and lithology of digital rock physics based on laboratory experiments. *Pet. Explor. Prod. Technol.* **2021**, *11*, 2113–2125. [[CrossRef](#)]
13. Tan, W.; Wang, P.; Wang, J.; Liu, J.; Ma, X. Mechanical Properties of Granite Under Uniaxial Compression Based on CT Technology. *J. Basic Sci. Eng.* **2020**, *28*, 1489–1498. [[CrossRef](#)]
14. Liu, H.; Wu, Z.; Zuo, Y.; Sun, W.; Zhu, Z.; Zheng, L.; Lou, Y.; Hou, Y. Fractal Study on Mesodamage Evolution of Three-Dimensional Irregular Fissured Sandstone. *Int. J. Geomech.* **2023**, *23*, 04023199. [[CrossRef](#)]
15. Mao, L.; Yuan, Z.; Lian, X.; Peng, R.; Liu, H. Measurement of 3D strain field in red stone sample under uniaxial compression with computer tomography and digital volume correlation method. *Chin. J. Rock Mech. Eng.* **2015**, *34*, 21–30. [[CrossRef](#)]
16. Wang, B.; Jin, A.; Zhao, Y.; Wang, H.; Liu, J.; Wei, Y.; Sun, H. Strength characteristics and 3D fracture evolution law of granite under unloading confining pressure. *J. Harbin Inst. Technol.* **2020**, *52*, 137–146. [[CrossRef](#)]
17. Gou, B.; Zhan, L.; Guo, J.; Zhang, R.; Zhou, C.; Wu, L.; Ye, J.; Zeng, J. Effect of different types of stimulation fluids on fracture propagation behavior in naturally fractured carbonate rock through CT scan. *J. Pet. Sci. Eng.* **2021**, *201*, 108529, ISSN 0920-4105. [[CrossRef](#)]
18. Zhang, Y.; Xu, Y.; Liu, X.; Yao, X.; Wang, S.; Liang, P.; Sun, L.B.; Tian, B.Z. Quantitative characterization and mesoscopic study of propagation and evolution of three-dimensional rock fractures based on CT. *Rock Soil Mech.* **2021**, *42*, 2659–2671. [[CrossRef](#)]
19. Zhao, Z.; Zhou, X.-P. 3D Digital Analysis of Cracking Behaviors of Rocks through 3D Reconstruction Model under Triaxial Compression. *J. Eng. Mech.* **2020**, *146*, 04020084. [[CrossRef](#)]
20. Wang, C.; Gao, A.; Shi, F.; Hou, X.; Ni, P.; Ba, D. Three-dimensional Reconstruction and Growth Factor Model for Rock Cracks under Uniaxial Cyclic Loading/Unloading by X-ray CT. *Geotech. Test. January* **2019**, *42*, 117–135. [[CrossRef](#)]
21. Lin, W.; Li, X.; Yang, Z.; Manga, M.; Fu, X.; Xiong, S.; Gong, A.; Chen, G.; Li, H.; Pei, L.; et al. Multiscale digital porous rock reconstruction using template matching. *Water Resour. Res.* **2019**, *55*, 6911–6922. [[CrossRef](#)]
22. Yan, W.; Golsanami, N.; Xing, H.; Li, S.; Chi, P. A Rapid Reconstruction Method of 3D Digital Rock with Strong Pore Connectivity. *Pure Appl. Geophys.* **2024**, *181*, 1601–1616. [[CrossRef](#)]
23. Zhang, X.; Fei, Z.; Zhong, W.; Li, T.; Wang, Z.; Jiang, L. Research and Implementation of Three-Dimensional Spatial Information Characterization and Visualization of Fractures in Deteriorated Sandstone. *Buildings* **2023**, *13*, 2418. [[CrossRef](#)]
24. Zhong, W. *Study on Damage Evolution Law of Sandstone Its Three-Dimensional Visualization*; Xihua University: Chengdu, China, 2023. [[CrossRef](#)]
25. Chu, H.; Chen, L.; Yang, X.; Wang, D.; Wei, H.; Sun, B. Experimental study on impact failure law of water-saturated granite with initial damage. *Explos. Shock Waves* **2024**, 1–16. [[CrossRef](#)]

26. Liu, J.; Zhou, Y.; Yang, H.; Fu, S.; Gu, Y. Energy and damage characteristics of shaft lining concrete subjected to impact. *J. China Coal Soc.* **2019**, *44*, 2983–2989. [[CrossRef](#)]
27. Yang, Y.; Li, Q.; Qiao, L. Review of SHPB dynamic load impact test characteristics and energy analysis methods. *Processes* **2023**, *11*, 3029. [[CrossRef](#)]
28. Dou, Q.B.; Wu, K.R.; Suo, T.; Zhang, C.; Guo, X.; Guo, Y.Z.; Guo, W.G.; Li, Y.L. Experimental methods for determination of mechanical behaviors of materials at high temperatures via the split Hopkinson bars. *Acta Mech. Sin.* **2020**, *36*, 1275–1293. [[CrossRef](#)]
29. Jin, J.F.; Li, X.-B.; Chang, J.-R.; Tao, W.; Qiu, C. Stress-strain curve and stress wave characteristics of rock subjected to cyclic impact loadings. *Explos. Shock Waves* **2013**, *33*, 613–619. [[CrossRef](#)]
30. Jin, J.; Fang, L.; Wang, Y.; Xiong, H.; Xiao, Y.; Peng, X. Experimental study on dynamic response characteristics of rocks under high water pressures and high stresses. *Chin. J. Rock Mech. Eng.* **2024**, *43*, 1821–1838. [[CrossRef](#)]
31. Zheng, G.; Xu, J.; Wang, P.; Fang, X.; Wang, P.; Wen, M. Static constitutive relation and dynamic mechanical properties of red sandstone with different water saturation. *J. Vib. Shock* **2018**, *37*, 31–37. [[CrossRef](#)]
32. Li, Z.; Ni, G.; Wang, Y.; Jiang, H.; Wen, Y.; Dou, H.; Jing, M. Semi-homogeneous model of coal based on 3D reconstruction of CT images and its seepage-deformation characteristics. *Energy* **2022**, *259*, 125044, ISSN 0360-5442. [[CrossRef](#)]
33. Chen, J. Study on Three-Dimensional Characterization and Permeability of Pores in Graded Discontinuous Gravel Soil. Master's Thesis, Guilin University of Technology, Guilin, China, 2023.
34. Xie, H.P. *Fractals in Rock Mechanics*, 1st ed.; Yang, L., Ed.; Science Press: Beijing, China, 1996; pp. 8–15. ISBN 7-03-005331-1.
35. Yang, R.; Xu, P. Fractal study of media damage under blasting loading. *J. China Coal Soc.* **2017**, *42*, 3065–3071. [[CrossRef](#)]

Disclaimer/Publisher's Note: The statements, opinions and data contained in all publications are solely those of the individual author(s) and contributor(s) and not of MDPI and/or the editor(s). MDPI and/or the editor(s) disclaim responsibility for any injury to people or property resulting from any ideas, methods, instructions or products referred to in the content.